Nonlinear hydrodynamic effects induced by Rayleigh surface acoustic wave in sessile droplets

M. Alghane,[1,2] B. X. Chen,[1,*] Y. Q. Fu,[1,3,†] Y. Li,[4] M. P. Y. Desmulliez,[1] M. I. Mohammed,[1] and A. J. Walton[4]

[1]*School of Engineering and Physical Sciences, Heriot-Watt University, Edinburgh EH14 4AS, United Kingdom*

[2]*Mechanical Engineering Department, Engineering College, University of Omar Al-Mukhtar, Al Bayda, Libya*

[3]*Thin Film Center, Scottish Universities Physics Alliance (SUPA), University of West of Scotland, Paisley PA1 2BE, Scotland*

[4]*Institute for Integrated Systems, Scottish Microelectronic Center, Institute for Integrated Micro and Nano Systems, School of Engineering, University of Edinburgh, Edinburgh EH9 3JF, United Kingdom*

(Received 18 November 2011; revised manuscript received 25 June 2012; published 9 November 2012)

We report an experimental and numerical characterization of three-dimensional acoustic streaming behavior in small droplets of volumes (1–30 μl) induced by surface acoustic wave (SAW). We provide a quantitative evidence of the existence of strong nonlinear nature of the flow inertia in this SAW-driven flow over a range of the newly defined acoustic parameter $F_{\mathrm{NA}} = \frac{F\lambda}{(\sigma/R_d)} \geqslant 0.01$, which is a measure of the strength of the acoustic force to surface tension, where F is the acoustic body force, λ is the SAW wavelength, σ is the surface tension, and R_d is the droplet radius. In contrast to the widely used Stokes model of acoustic streaming, which generally ignores such a nonlinearity, we identify that the full Navier-Stokes equation must be applied to avoid errors up to 93% between the computed streaming velocities and those from experiments as in the nonlinear case. We suggest that the Stokes model is valid only for very small acoustic power of $\leqslant 1$ μW ($F_{\mathrm{NA}} < 0.002$). Furthermore, we demonstrate that the increase of F_{NA} above 0.45 induces not only internal streaming, but also the deformation of droplets.

DOI: 10.1103/PhysRevE.86.056304 PACS number(s): 47.10.ad, 43.25.Fe, 47.35.−i, 47.55.−t

I. INTRODUCTION

Acoustic streaming, the motion of bulk fluid, arises from the interaction of acoustic waves with fluids [1]. Associated with standing waves, this phenomenon was first observed in 1831 by Faraday [2], and theoretically analyzed by Rayleigh in 1848 [1], in which the dissipation of the acoustic energy was considered within the boundary layer of the solid surfaces (vortexlike streaming) [3]. In 1948, Eckart [4] presented an interesting acoustic streaming theory and was able to derive an expression for the streaming velocity in the one-dimensional case. Eckart's theory was based on the propagation of the sound wave pressure away from the ultrasound source and its exponential attenuation in the body of fluid volume. His expression was derived by applying the method of successive approximations to the Navier-Stokes (NS) equations. The hydrodynamic nonlinearity term was ignored by assuming its value to be negligible [5].

Nyborg [6] extended Eckart's theory to describe a streaming phenomenon induced by an ultrasonic plane wave and concluded that the mean streaming flow was due to the loss of acoustic momentum. According to Nyborg's theory of acoustic streaming [6,7], the flow field can be obtained by solving the stationary Stokes equations of incompressible flow,

$$\mathbf{0} = \frac{1}{\rho}\boldsymbol{F} - \nabla \boldsymbol{P} + \nu\nabla^2\boldsymbol{U}, \quad \nabla \cdot \boldsymbol{U} = 0, \tag{1}$$

where U is the streaming velocity, P is the kinematic pressure, ν is the kinematic viscosity, and ρ is the fluid density. F is the acoustic body force due to the presence of the sound source [6]. As can be seen in Eq. (1), the nonlinear term, i.e., $(U \cdot \nabla)U$, has not been included based on the assumption that $\boldsymbol{U} \ll C_w$, where C_w represents the sound wave velocity in the fluid.

In this study, we consider the Eckart type acoustic streaming generated by a high frequency (~60 MHz) surface acoustic wave (SAW) in droplets with volumes ranging from 1 to 30 μl. When a liquid either in bulk or a droplet lies on the propagation path of an emitted SAW, the SAW changes its mode into a leaky SAW (LSAW) and damps exponentially when reaching the liquid. Longitudinal pressure waves are then created and propagate into the fluid at a Rayleigh angle $\theta_R = \sin^{-1}\frac{C_w}{C_s}$ [8], as shown in Fig. 1(a), where C_s is the SAW velocity in substrate. These radiated pressure waves induce an acoustic body force, Eq. (2), in the fluid medium [8–10], which results in a bulk liquid circulation within the droplet [11],

$$\boldsymbol{F} = -\rho(1+\alpha^2)^{3/2}A^2\omega^2 k_i \exp 2(k_i x + \alpha k_i y). \tag{2}$$

Here, ω is the angular frequency, k_i is the wave number, α is the attenuation constant, and A is the SAW amplitude at the interaction point, as identified by an empirical correlation,

$$\frac{A}{\lambda} = 8.15 \times 10^{-6} P_D^{0.225} + 5 \times 10^{-6} P_D^{0.8}, \tag{3}$$

where P_D is the radio frequency (rf) power applied to the SAW device in watts, and λ is the SAW wavelength [12,13].

Recently, surface acoustic wave (SAW) based microfluidics has been utilized in numerous engineering applications [14]. Various streaming phenomena, including mixing, pumping, ejection, and particles concentration, have been reported for liquid droplets located within the propagation path of a SAW device [12,15–19]. Meanwhile, as a result of the rapid progress in the SAW microfluidics [14], many studies have been done to provide numerical solutions for the SAW-driven microfluidics. Some of the examples include (a) studies on the characterization of flow patterns and microfluidic mixing via SAW in two-dimensional (2D) flows [11,20], (b) computation of apparent free-surface deformation of

*Corresponding author: b.chen@hw.ac.uk

†Corresponding author: richard.fu@uws.ac.uk

stationary droplets [21], and (c) analysis of microparticle accumulation in stationary microchannels flow [22] under the SAW excitation. Most studies of the SAW-driven fluids used the acoustic body force approach based on the Stokes model of Nyborg's theory [6]. For instance, Franke *et al.* [23] reported that the nonlinearity (inertial) effects arising from SAW propagation in fluid medium were nearly negligible and the Stokes model was applicable, due to the small geometries of droplets.

However, only a few studies have been reported on the effects of hydrodynamics nonlinearity in acoustic streaming [24–26], and even these studies were limited to ultrasonic standing waves, rather than SAW. For example, Lighthill [27,28] discussed the effects of hydrodynamic nonlinearity on acoustic streaming of standing wave generated by a cylindrical resonator in an unbounded fluid medium, and concluded that the nonlinearity effects of fluid inertia were significant in all noticeable acoustic streaming examples. Nevertheless, the nonlinear term of flow inertia in the SAW studies was normally ignored [29], even for very high SAW powers up to 6×10^4 μW [30–33]. In this paper, we present a systematic experimental and numerical study concerning the effects of the hydrodynamic nonlinearity on the SAW-driven fluids.

II. METHODS

In this study, the characteristics of fluid flow induced by a Rayleigh SAW in sessile droplets are investigated using both the numerical simulations and experimental measurements.

A. Experiment

In our experimental studies, the SAW devices were fabricated on 128° YX black $LiNbO_3$ substrates by sputtering 200-nm-thick aluminum to form the interdigitated transducer (IDT) electrodes. A spin-coated CYTOP®(Asahi Glass Co., Ltd., Tokyo, Japan) layer was prepared to make the surface hydrophobic, as the surface of the $LiNbO_3$ wafers is originally hydrophilic, as shown by the schematic illustration in Fig. 1(a). The details of the SAW device fabrication have been documented elsewhere [34]. In this study, we used an IDT with a wavelength of $\lambda = 64$ μm and fundamental frequency $f \approx 60$ MHz. The SAW was launched by applying an rf signal, P_D, to the IDTs using a standard signal generator (MI 2019A) amplified by an MI TF2175 rf power amplifier. Water droplets (1–30 μl) were loaded symmetrically with the SAW propagation path, using a micropipette. For the measurements of the streaming velocities, polystyrene particles with an average diameter of 6 μm were placed inside the water droplet, and their adjective motion was recorded using a high speed camera (Kodak Motion Corder Analyzer, 600 fps).

B. Modeling details

The computational analysis was performed using the finite volume method (FVM), and OpenFOAM-1.6 CFD code (OpenCFD Ltd.) was used for our model development. The induced flow streaming in the liquid droplet was assumed to be governed by the laminar incompressible 3D Navier-Stokes (NS) equations, which are driven by an external acoustic force F [3],

$$\frac{\partial \boldsymbol{U}}{\partial \boldsymbol{t}} + (\boldsymbol{U} \cdot \nabla)\boldsymbol{U} = \frac{1}{\rho}\boldsymbol{F} - \nabla \boldsymbol{P} + \nu \nabla^2 \boldsymbol{U}, \quad \nabla \cdot \boldsymbol{U} = 0 \quad (4)$$

In our numerical analysis, rf powers were applied in range $P_D \leqslant 16$ mW, to keep the droplet in its original shape without inducing significant distortion. Consequently, stress-free boundary conditions can be applied at the droplet-air interface. The preliminary results and calibration of our code have been reported in Refs. [35,36]. Only for the analysis of linearized hydrodynamic model, the nonlinear term $(U \cdot \nabla)U$ in Eq. (4) was ignored, which gives a transient version of the Stokes model, Eq. (1). In this study, all the numerical cases were run to the steady state, and these results are discussed in the following sections.

III. RESULTS AND DISCUSSION

A. Dimensionless parameters

The main parameters that govern the system of SAW-driven droplets are those of the flow field of the droplet hydrodynamics, and those of the sound field that generates either a flow inside the droplets or distortion of droplets shape. The hydrodynamics parameters include the streaming velocity U (m/s), the fluid viscosity ν (m^2/s), and the droplet radius R_d (m), as characterized by the Reynolds number $\mathrm{Re} = \frac{U R_d}{\nu}$. Another parameter is the surface tension σ (N/m), a force that plays a significant role against the SAW force to retain the original shape of the droplet. The characteristic parameters of the sound field are the SAW wave amplitude A (m), Eq. (3), and the SAW wavelength λ (m) that measures the propagation depth of SAW into the droplet fluid [37]. These two parameters are involved in Eq. (2) of the acoustic body force F (N/m^3).

In this study, we found from both the experimental and numerical simulation results that the driving SAW characteristics can be described by a dimensionless parameter of normalized acoustic force F_{NA}, as defined by

$$F_{\mathrm{NA}} = \frac{F\lambda}{\sigma / R_d}. \quad (5)$$

The proposed parameter of F_{NA} represents the ratio of the acoustic force (e.g., measured at a point where the SAW enters the droplet) per unit area, $F\lambda$, to the surface tension per unit length, σ/R_d. The new dimensionless parameter of the F_{NA} proposed in this study can be used to describe not only the characteristics of acoustic wave field, but also the hydrodynamics of the SAW-driven droplets including the deformation mechanism. These two dimensionless parameters, i.e., F_{NA} and Re, are used in the analysis and discussion of hydrodynamics of droplets induced by SAW in this paper.

B. Influences of fluid inertia on streaming phenomena

1. Reynolds number

Effects of hydrodynamics nonlinearity on the streaming phenomenon are discussed in terms of the steady state Re of induced internal flow dynamics by a SAW-droplet coupling, using a moderate range of a normalized acoustic force, F_{NA} [Eq. (5)], as shown in Fig. 1.

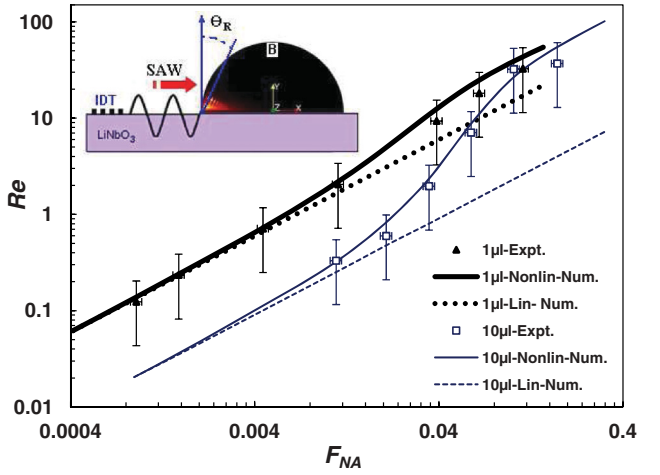

(a)

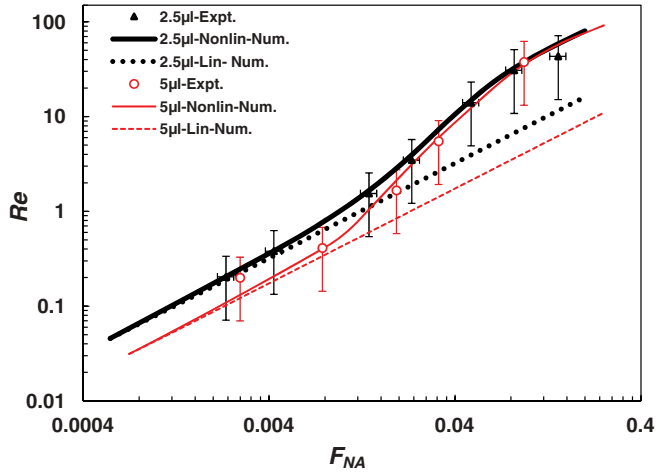

(b)

FIG. 1. (Color online) Effects of hydrodynamic nonlinearity in the relation between the steady state Reynolds numbers Re and F_{NA}, using 128° YX-$LiNbO_3$ SAW device with 0.5-mm aperture excited by a frequency of 60.4 MHz; (a) results for 1- and 10-μl droplets; and (b) results for 2.5- and 5-μl droplets. Solid and broken lines represent the nonlinear and linear numerical results, respectively. The markers denote the experimental data.

As shown in Figs. 1(a) and 1(b) by the relation between the Reynolds number and F_{NA} parameter in log-log scale, when $F_{NA} \leqslant 0.002$ ($P_D \leqslant 1$ μW), the results from the Stokes model, Eq. (1), and the full NS model, Eq. (4), give very good agreement in comparison with experimental measurements. This is based on an error analysis using defined deviation of $\varepsilon = |I - \frac{\mathrm{Re}_l}{\mathrm{Re}_{nl}}| \leqslant 5.0 \times 10^{-2}$, where Re_l and Re_{nl} are the Reynolds number of linearized and nonlinearized cases, respectively. This means that the linearization assumption is valid only for the simulation of acoustic streaming at very low SAW powers of the microwatt range. This validation can also be identified by the associated Reynolds number with $\mathrm{Re} < 1$ if and only if the droplets size is small enough, such as for the droplet volumes of 1.0 or 2.5 μl used in this study in Figs. 1(a) and 1(b), respectively. It should be noted that the condition of $\mathrm{Re} < 1$ that has been imposed in most studies of employing the linear assumption [29] is not applicable for larger droplet volumes, such as 5 or 10 μl in this study. The results in Fig. 1 show that the flow inertia does appear, and becomes negligible only at a condition of $\mathrm{Re} \ll 1$. However, when the SAW power increases, $F_{NA} \geqslant 0.01$ (or $P_D \geqslant 20$ μW), the difference between the Stokes model results and experimental data becomes significant, and can be as high as 90%, especially for the larger droplets. Meanwhile, this difference is only about 10% for the NS model as shown in Figs. 1(a) and 1(b). This closer agreement with experimental data is due to the contribution of flow inertia, where the increase in the F_{NA} (or SAW power) enhances the role of the hydrodynamic nonlinearity term in the nonlinear NS model in Eq. (4); which becomes too large to be ignored.

Additionally, in the nonlinear region, it is clearly visible from the experimental and the nonlinear NS modeling results in Figs. 1(a) and 1(b) that the differences in the value of Re for the two droplets sizes decrease gradually with an increase of

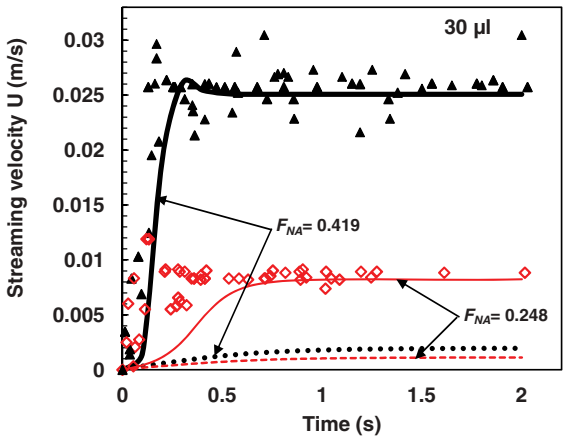

(a)

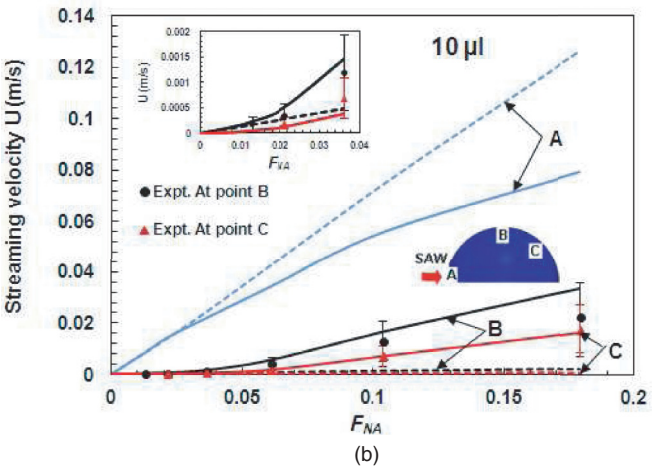

(b)

FIG. 2. (Color online) Hydrodynamic nonlinearity effects on (a) the transient streaming velocity of a 30-μl droplet measured at point B, using 128° YX-$LiNbO_3$ SAW device with 62-MHz frequency, 2-mm aperture at different F_{NA}; (b) the streaming velocity as a function of F_{NA} for a 10-μl droplet using a 0.5-mm aperture SAW device driven at 60.4 MHz. Solid and broken lines represent the nonlinear and linear numerical results, respectively. The markers are the experimental measurements.

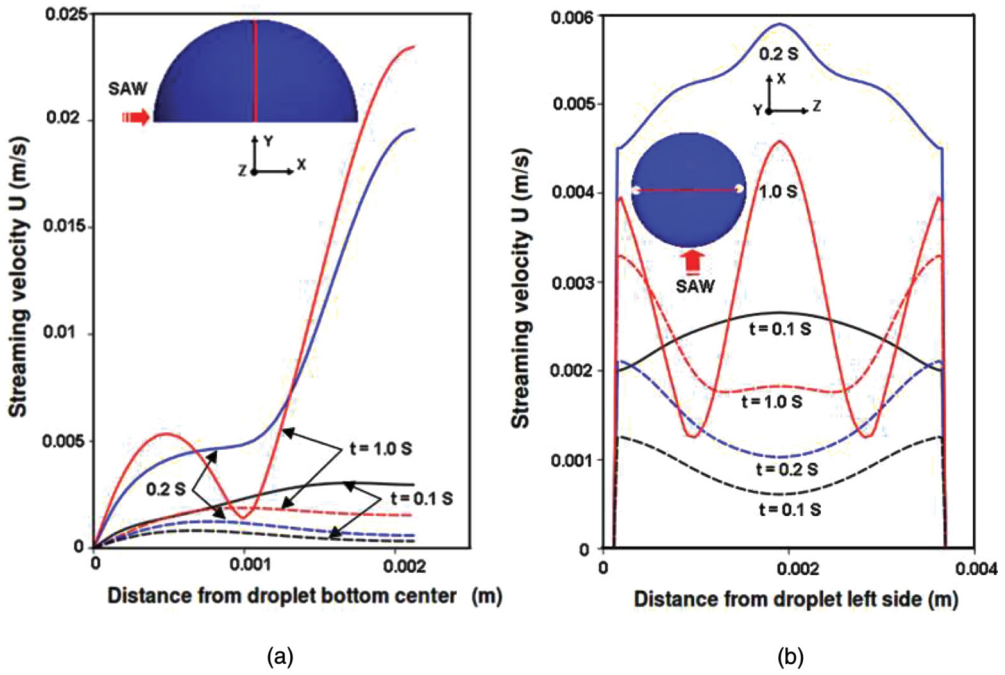

FIG. 3. (Color online) Simulated streaming velocity profiles for 20-μl droplet, using SAW device with 2.5-mm aperture, 62-MHz frequency, and F_{NA} of 0.366; (a) along the Y axis; (b) along the Z axis at a 1200-μm height from the droplet bottom. Solid and broken lines represent the nonlinear and linear cases, respectively.

the acoustic power, and become considerably smaller as long as $F_{NA} > 0.05$. In contrast, the Stokes model results show a fixed difference in the value of Re with variation in the drops volumes for the whole range of F_{NA} values, a situation not confirmed by the experimental data.

2. *Flow development and streaming velocity*

In order to identify the role of nonlinear term in SAW acoustic streaming, the transient streaming velocity at the top center of a 30-μl droplet is examined in Fig. 2(a) by comparing both simulation and experimental results. Results show that the droplet internal flow has been accelerated quickly to a steady velocity within one second, with higher F_{NA} of 0.419. Increasing the F_{NA} (or rf power) reduces this initial time due to the increase in the SAW momentum delivered to the fluid. As shown in Fig. 2(a), the values of streaming velocities from the nonlinear NS model are in good agreement with the experimental data. On the other hand, the Stokes model results are one order of magnitude less than those of experiments. Furthermore, the discrepancy between the steady state experimental and numerical results for an F_{NA} of 0.248 is 87.4%, and becomes 92.5% for an F_{NA} of 0.419, when flow inertia (hydrodynamic nonlinearity) is ignored. Conversely this discrepancy is only 0.47% and 1.37%, respectively, when the hydrodynamics nonlinearity is taken into account. Also, at a steady state stage, the deviation of the velocity for the two power cases is ~16 mm/s, both from the experimental and nonlinear numerical results using the NS model, compared with only ~0.846 mm/s in the linear case (i.e., using Stokes model).

Figure 2(b) shows both experimental and simulations results of the streaming velocity as a function of F_{NA} for a 10-μl droplet at three observation points; i.e., point A is close to the SAW source, point B is at the top center of the droplet, and point C is far away from the SAW source. However, due to the difficulties and challenges with capturing the flow field near the SAW source during the experiments, only the numerical results are presented for point A. It can be observed once again that the importance of the fluid-hydrodynamics nonlinearity becomes more significant with the increase of the SAW power, due to the increase of the streaming velocity, where the inertial forces become dominant. The linear approximation using the Stokes model results in a higher streaming velocity near the SAW source (point A) and a much lower reading at regions away from the SAW source (B and C).

The role of the nonlinear term on the droplet-acoustic streaming can be further illustrated by taking the case of a 20-μl droplet and examining the velocity distribution in three dimensions. The velocity distribution was measured along two axes through the droplet, i.e., the vertical Y axis shown in Fig. 3(a), and the horizontal Z axis at a height of 1200 μm from the bottom of the droplet shown in Fig. 3(b). Figure 3(a) shows that at an early stage (< 0.1 s), both the nonlinear and linear approximations have similar velocity profiles. However, as the flow develops, the differences between the two profiles become significant. This is also true for the velocity profiles along the horizontal Z axis, as can be observed in Fig. 3(b). Figure 3(a) shows that the value of steady state streaming velocity using the Stokes model is less than that using the NS model by about 93% at the top of the droplet, and about 60% less at the center of the droplet, as shown in Fig. 3(b). These results clearly show the consequences of ignoring the hydrodynamic nonlinearity of flow inertia in the predictions of SAW acoustic streaming, from both qualitative and quantitative points of view.

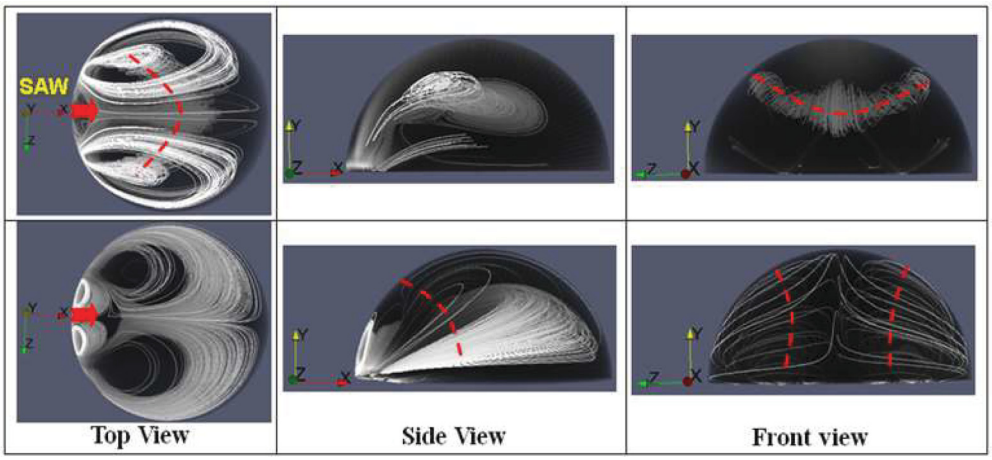

FIG. 4. (Color online) Simulated streaming patterns for 20-μl droplet, using SAW device with 2.5-mm aperture, 62-MHz frequency, and F_{NA} of 0.366. The upper and lower row represents the nonlinear and linear cases, respectively. Broken lines represents axis of rotation.

3. *Flow patterns of acoustic streaming*

For qualitative illustration, the simulated flow patterns inside the droplet from the two models are presented in Fig. 4, i.e., the Stokes and the NS model. The top row in Fig. 4 shows that the butterfly flow pattern rotates around one elliptical axis of rotation through the droplet center when the NS model is applied, which has been verified by experimental observations [35,36]. In contrast, when the Stokes model is used for the simulations, the flow pattern only rotates around the double vertical axis with two small vortices near the SAW source, as shown in the second row in Fig. 4, which does not agree with the experimental observations. The precise identification of the acoustic streaming patterns is required when designing efficient lab-on chip SAW-mixing devices with a minimal applied rf power. For instance, applying the Stokes model (ignoring the nonlinear term) to model SAW mixing of bioparticles inside relatively larger droplets (such as 20 μl simulated in this study) will predict that a very large power is needed to get the uniform butterfly flow pattern with efficient flow rotation, as shown in the first row of Fig. 4. Such a large recommended power is not necessary as evidenced by experiments carried out from this paper. It is also well known that the application of high acoustic powers would cause significant acoustic heating effects, which would be detrimental to the biosensing process or could potentially destroy temperature sensitive biological samples [38,39].

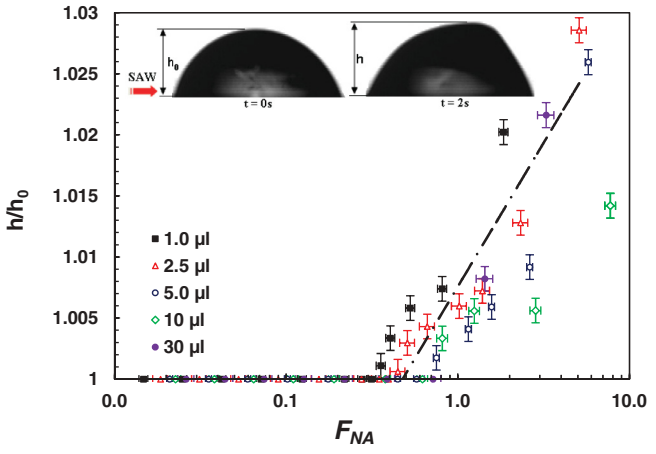

FIG. 5. (Color online) Normalized droplet height as a function of the normalized driving force (F_{NA}), for different droplet volumes, using 128° YX-$LiNbO_3$ SAW devices with 0.5-mm aperture excited by a frequency of 60.4 MHz; dashed line stands for trend line.

C. Droplet deformation

Additionally, we demonstrate here that the new F_{NA} parameter can also be employed to identify the induced droplets deformation by SAW. The detailed experimental measurements of the droplet height ratio h/h_0 as a function of the F_{NA}, seen in Fig. 5, show that the droplet deformation with a significant change in its height h from initial height h_0 can be clearly predicted at $F_{NA} > 0.45$. Although the detailed mechanism of SAW-induced droplet deformation is beyond the scope of this paper, we would like to give a brief explanation. As we suggested earlier, the acoustic power emitted by the SAW into the droplets is dominated by the balance between the SAW acoustic force and surface tension force, as characterized by the values of the F_{NA}. When $F_{NA} > 0.45$, SAW-droplet coupling induces hydrodynamic forces and pressure [21,40], which cannot be balanced by surface tension, and thus results in droplet distortion into an asymmetrical shape, as shown in Fig. 5.

IV. CONCLUSIONS

In conclusion, by introducing a new dimensionless acoustic force parameter $F_{NA} = \frac{F\lambda}{(\sigma/R_d)}$ in our analysis for the SAW-induced acoustic streaming inside the droplets (1–30 μl), we are able to present qualitative and quantitative comparisons between the experimental data and numerical simulation results. This provides strong evidence of the existence of significant hydrodynamics nonlinearity in this system, over a range of the values of F_{NA}. Therefore, we classify the flow within droplets into three flow regimes or modes: (1) the viscous dominant mode, when $F_{NA} \leqslant 0.002$, where the widely reported Stokes model of Nyborg's theory [6] is applicable;

(2) the inertia dominant mode, when $F_{NA} \geqslant 0.01$, where the full 3D NS equations must be applied in order not to cause a large error in streaming velocity predictions, which could be as large as $\sim$93%; (3) the droplet deformation or movement mode, with a threshold $F_{NA} \approx 0.45$, above which the droplet deforms. In brief, we have demonstrated that the hydrodynamic nonlinearity plays a significant role in most noticeable SAW acoustic streaming of droplets actuation (e.g., Re $\geqslant$ 1).

ACKNOWLEDGMENTS

We acknowledge the financial support from the Innovative electronic Manufacturing Research Center (IeMRC) through the EPSRC funded flagship project SMART MICROSYSTEMS (FS/01/02/10), the Carnegie Trust Funding, the Royal Society of London (Research Grant No. RG090609), and the Royal Society of Edinburgh.

[1] L. Rayleigh, Philos. Trans. R. Soc. London **175**, 1 (1884).
[2] M. Faraday, Philos. Trans. R. Soc. London **121**, 299 (1831).
[3] H. Mitome, Electron. Commun. Jpn. Part 3 (Fund. Electron. Sci.) **81**, 1 (1998).
[4] C. Eckart, Phys. Rev. **73**, 68 (1948).
[5] M. K. Aktas and B. Farouk, J. Acoust. Soc. Am. **116**, 2822 (2004).
[6] W. L. Nyborg, in *Physical Acoustics*, edited by W. P. Mason (Academic, New York, 1965), p. 265.
[7] W. L. Nyborg, in *Nonlinear Acoustics*, edited by M. F. Hamilton (Academic, New York, 1998), p. 207.
[8] S. Shiokawa, Y. Matsui, and T. Ueda, in *Proceedings of the Ultrasonics Symposium, 1989, Montreal, Quebec*, Vol. 1 (IEEE, New York, 1989), pp. 643–646.
[9] S. Shiokawa, Y. Matsui, and T. Moriizumi, Jpn. J. Appl. Phys. **28**, 126 (1989).
[10] S. Shiokawa, Y. Matsui, and T. Ueda, Jpn. J. Appl. Phys. **29**, 137 (1990).
[11] T. Frommelt, M. Kostur, S. Wenzel-Schäfer, P. Talkner, P. Hänggi, and A. Wixforth, Phys. Rev. Lett. **100**, 034502 (2008).
[12] K. Chono, N. Shimizu, Y. Matsui, J. Kondoh, and S. Shiokawa, Jpn. J. Appl. Phys. **43**, 2987 (2004).
[13] A. Sano, Y. Rlatsui, and S. Shiokawa, in *Proceedings of the Ultrasonics Symposium, 1997, Toronto, Ontario*, Vol. 1 (IEEE, New York, 1997), pp. 467–470.
[14] J. Friend and L. Y. Yeo, Rev. Mod. Phys. **83**, 647 (2011).
[15] R. P. Hodgson, M. Tan, L. Yeo, and J. Friend, Appl. Phys. Lett. **94**, 024102 (2009).
[16] R. V. Raghavan, J. R. Friend, and L. Y. Yeo, Microfluid. Nanofluid. **8**, 73 (2009).
[17] A. Sano, Y. Matsui, and S. Shiokawa, Jpn. J. Appl. Phys. **37**, 2979 (1998).
[18] W. Tseng, J. Lin, W. Sung, S. Chen, and G. Lee, J. Micromech. Microeng. **16**, 539 (2006).
[19] A. Wixforth, J. Assoc. Lab. Autom **11**, 399 (2006).
[20] T. Frommelt, T. D. Gogel, M. Kostur, P. Talkner, and P. Hanggi, IEEE Trans. Ultrason. **55**, 2298 (2008).
[21] M. Schindler, P. Talkner, and P. Hanggi, Phys. Fluids **18**, 103303 (2006).
[22] M. Schindler, P. Talkner, M. Kostur, and P. Hänggi, Physica A **46**, 385 (2007).
[23] T. A. Franke and A. Wixforth, Chem. Phys. Chem. **9**, 2140 (2008).
[24] T. Kamakura, K. Matsuda, Y. Kumamoto, and M. A. Breazeale, J. Acoust. Soc. Am. **97**, 2740 (1995).
[25] R. M. Moroney, R. M. White, and R. T. Howe, Appl. Phys. Lett. **59**, 774 (1991).
[26] M. W. Thompson, A. A. Atchley, and M. J. Maccarone, Appl. Phys. Lett. **117**, 1839 (2005).
[27] J. Lighthill, *Internal Waves in Fluids* (Cambridge University Press, Cambridge, England, 1978).
[28] J. Lighthill, J. Sound Vib. **61**, 391 (1978).
[29] M. K. Tan, J. R. Friend, O. K. Matar, and L. Y. Yeo, Phys. Fluids **22**, 112112 (2010).
[30] S. K. R. S. Sankaranarayanan and V. R. Bhethanabotla, J. Appl. Phys. **103**, 064518 (2008).
[31] S. K. R. S. Sankaranarayanan and V. R. Bhethanabotla, IEEE Trans. Ultrason. Ferroelectr. Freq. Control **56**, 631 (2009).
[32] S. K. R. S. Sankaranarayanan, S. Cular, V. R. Bhethanabotla, and B. Joseph, Phys. Rev. E **77**, 066308 (2008).
[33] S. K. R. S. Sankaranarayanan, R. Singh, and V. R. Bhethanabotla, J. Appl. Phys. **108**, 104507 (2010).
[34] X. Y. Du, M. E. Swanwick, Y. Q. Fu, J. K. Luo, A. J. Flewitt, D. S. Lee, S. Maeng, and W. I. Milne, J. Micromech. Microeng. **19**, 035016 (2009).
[35] M. Alghane, B. X. Chen, Y. Q. Fu, Y. Li, J. K. Luo, and A. J. Walton, J. Micromech. Microeng. **21**, 015005 (2010).
[36] M. Alghane, Y. Q. Fu, B. X. Chen, Y. Li, M. P. Y. Desmulliez, and A. J. Walton, J. Appl. Phys. **109**, 114901 (2011).
[37] R. M. Arzt, E. Salzmann, and K. Dransfeld, Appl. Phys. Lett. **10**, 165 (1967).
[38] J. Kondoh, N. Shimizu, Y. Matsui, M. Sugimoto, and S. Shiokawa, in *Sensors, Irvine, CA* (IEEE, New York, 2005).
[39] T.-D. Luong, V.-N. Phan, and N.-T. Nguyen, Microfluid. Nanofluid. **10**, 619 (2011).
[40] P. Brunet, M. Baudoin, O. B. Matar, and F. Zoueshtiagh, Phys. Rev. E **81**, 036315 (2010).